Hydrogen implantation-induced blistering in diamond : towards diamond layer transfer by the Smart CutTM technique

Cédric Masante, Jon de Vecchy, Frédéric Mazen, Frederic Milesi, Léa Di Cioccio, Julien Pernot, Fernando Lloret, Daniel Araujo, José Carlos Pinero, Névine Rochat, et al.

HAL Id: cea-03714349

https://cea.hal.science/cea-03714349

Submitted on 5 Jul 2022

Hydrogen implantation-induced blistering in diamond: Toward diamond layer transfer by the Smart Cut™ technique

C. Masante [a], J. de Vecchy [a], F. Mazen [a], F. Milesi [a], L. Di Cioccio [a], J. Pernot [b], F. Lloret [c], D. Araujo [d], J.C. Pinero [e], N. Rochat [a], F. Pierre [a], F. Servant [a], J. Widiez [a,*]

[a] Univ. Grenoble Alpes, CEA, Leti, F-38000 Grenoble, France
[b] Univ. Grenoble Alpes, CNRS, Institut Néel, Grenoble 38000, France
[c] Department of Applied Physics, University of Cádiz, Spain
[d] Department of Materials Science, University of Cadiz, Puerto Real, Cadiz, Spain
[e] Departamento de Didáctica, área de Matemáticas, Universidad de Cádiz, 11510, Spain

ARTICLE INFO

ABSTRACT

The effect of H$^+$ implantation and annealing of diamond (100) monocrystalline substrates has been studied by ToF-SIMS, cathodoluminescence, transmission spectroscopy and TEM. Blistering conditions suitable for the Smart Cut™ technology have been identified in monocrystalline diamond, using two sets of hydrogen implantation and annealing. A first hydrogen implantation followed by a first annealing leads to amorphization of a buried layer without hydrogen exodiffusion. Blisters and exfoliations appear at the surface of the diamond samples, after a second hydrogen implantation inside the pre-amorphized diamond layer and a final annealing, as evidenced by TEM and optical microscopy. Demonstration of hydrogen-induced blistering is a major step to adapt the Smart Cut™ process on diamond material. This process is compatible with wafer bonding before the second annealing and therefore open the way for thin diamond layer transfer on a bonded receiver wafer, still not achieved to date.

1. Introduction

Diamond based devices are attracting a lot of interest for future generations of ultra-wide band gap semiconductor power devices. Diamond devices stand out for their efficiency at high voltage, high temperature and in harsh environments, thanks to its outstanding electronic and thermal properties. However, despite constant efforts to increase the substrate surface area, the vast majority of device demonstrations are made on mm^2 sized diamond plates. The two preferred method to grow diamond are High Pressure High Temperature (HPHT) and Chemical Vapor Deposition (CVD). These methods can produce low defect density diamonds, but are not suitable to achieve wafer scale substrates, because of the very low growth speed and the small size of the diamond seeds. Hence, the price for electronic grade multisectorial plates is much higher than other wide band gap material such as GaN, SiC and Ga$_2$O$_3$, with low availability of substrates of more than 2 cm^2. Also, heteroepitaxy is being used to produce large monocrystalline diamond substrates [1]. But the resulting defect density in the grown diamond layer is still too high from a device fabrication standpoint. Achieving wafer size

electronic grade diamond layers is key toward efficient device development and successful industrialization. Most device fabrication lines do not accept less than 2 in. wafers.

A promising approach to overcome wafer dimension and cost issues is the use of a thin layer transfer technology. Such technique allows economy of matter by transferring a thin layer on a cheaper handling substrate. By using multiple layer transfer, large substrate paving can be achieved, promoting diamond access to standardized microelectronics equipment. Realization of free standing diamond films has already been demonstrated in the past. The most reported technique uses the selective etching of a graphite sacrificial layer created by ion implantation [2–5]. This technique has been improved over the years [6–8] and is still used today [9]. These methods are however limited by the long etching time of the graphite layer and have poor compatibility with wafer bonding technologies.

The most widely used semiconductor thin layer transfer technique is the Smart Cut™ technology [10]. It first allowed Soitec to produce Silicon-On-Insulator wafers [11] and has been since adapted to other wide band gap semiconductor materials such as silicon carbide [12] or

gallium nitride [13], but not yet to diamond. This technique uses ion implantation, most of the time light ions such as hydrogen, to create buried nano-cavities inside the material, called platelets in the case of silicon [14]. The implanted wafer is then bonded to a handle substrate and a final annealing activates H_2 formation that feeds the cavities and makes them expand. Under the interface mechanical stress due to the bonded substrate, the cavities widen and coalesce laterally, forming microcracks and a final fracture that quickly spreads to whole wafer, allowing separation of the thin film. Compared with graphite selective etching technique, the splitting time is faster and not size dependent, i.e. this technique can easily be applied to larger substrates without downsides.

In the absence of a bonded handle substrate, gas-fed cavities are free to expand horizontally and vertically, thus deforming the substrate surface causing bubbles to appear. This phenomenon is called blistering. Finding implantation and annealing conditions leading to blistering, is a key step toward the demonstration of the Smart Cut™ process. Combined with a suitable wafer bonding technique, blistering conditions are necessary to achieve the layer transfer after the final annealing. Blistering literature in diamond is sparse and only some conditions have been reported using hydrogen [15–21]. They often require annealing temperatures over ≥1300 °C, not suitable with standardized production and limiting potential bonding techniques due to coefficient of linear thermal expansion mismatch. Suk et al. [22] reported the most convincing blistering conditions up to now. They introduced a pre-amorphization step by carbon implantation and annealing, to create a buried graphite-like layer which is then implanted with hydrogen. After a final 850 °C annealing, they obtained the delamination of a 2.3 μm thick diamond layer. However, this process uses carbon ion implantation which requires large implantation energies in the MeV range to preserve the near-surface crystallinity. Hence, the achievable film thickness is in the micrometer scale. We thus propose in this work to realize the pre-amorphization step using hydrogen. It is well known that light ion implantation induced damage is more concentrated at the end-of-range, making possible the realization of higher quality, thinner film transfers. Hydrogen implantation conditions and annealing leading to a suitable graphite-like layer, and then to blistering, are thus to be determined. Pinero et al. [23] previously published a TEM study of hydrogen implantation amorphization of diamond. In this work, we further characterize the evolution of diamond upon ion induced amorphization. In the first part, the experimental process flow will be detailed. The second part will deal with the diamond pre-amorphization after the first combination of ion implantation and annealing. In the third part, the blistering phenomenon induced after the whole process, using only hydrogen implantation, will be demonstrated and characterized.

2. Experimental

Three IIa (100) HPHT $4 \times 4 \times 0.5$ mm^3 diamond plates from New Diamond Technology (NDT) and one IIa (100) CVD $3 \times 3 \times 0.3$ mm^3 diamond plate from LakeDiamond have been implanted and annealed following the conditions described in Table I. The whole process is depicted in Fig. 1. The three NDT samples have been first used to study the pre-amorphization conditions by performing hydrogen implantation (step 1) at 60 ke V with doses of 5×10^{16} cm^{-2}, 1.4×10^{17} cm^{-2} and 3×10^{17} cm^{-2}. Referred respectively as low dose (LD), medium dose (MD) and high dose (HD). All three samples were then annealed (step 2) during 1 h at 1000 °C under vacuum (1×10^{-8} mbar). After the step 2 annealing, a color change was observed indicating a structural modification of the implanted layer, but no significant blistering was obtained. Two localized blisters were nonetheless observed on the HD sample, with diameters of approximately 215 μm and 250 μm. The induced maximum vacancy density simulated by SRIM [24] is given in Table I. The LakeDiamond sample was then used to find suitable blistering conditions with the full process (steps 1 to 4). Thanks to a hard mask,

Table I

H$^+$ doses and their associated vacancy density (D$_v$), simulated by SRIM. LD refers to "low dose", MD to "medium dose", HD to "high dose", B1 to "Blistering 1" and B2 to "Blistering 2".

	Steps 1 and 2 study			Blistering study (step 4)	
	LD	MD	HD	B1	B2
Dose 1 (cm^{-2})	5.0×10^{16}	1.4×10^{17}	3.0×10^{17}	1×10^{17}	1.5×10^{17}
D$_v$ 1 (cm^{-3})	2.0×10^{22}	5.6×10^{22}	1.2×10^{23}	4×10^{22}	6×10^{22}
Dose 2 (cm^{-2})				2.3×10^{17}	2.3×10^{17}
D$_v$ 2 (cm^{-3})				9.2×10^{22}	9.2×10^{22}

this substrate was hydrogen implanted and annealed in the same conditions as the NDT samples, but with two different doses, 1×10^{17} cm^{-2} and 1.5×10^{17} cm^{-2}, referred respectively as B1 and B2. Following the first 1000 °C annealing, another set of implantation and annealing was performed on the LakeDiamond sample with a fixed dose of 2.3×10^{17} cm^{-2} (see Table I) at the same energy, voltage parameters and annealing conditions used previously (step 3 and 4 in Fig. 1). After the 1000 °C step 4 annealing, significant blistering was only observed with B2 condition. A large portion of the surface was covered with bubbles and exfoliation.

The implanted hydrogen concentration is tracked using time of flight secondary ion mass spectroscopy (ToF-SIMS) after steps 1 and 2. Hydrogen-related or point defects created during steps 1 and 2 were studied by cathodoluminescence and optical transmission. Finally, the blistered sample formed after step 4 annealing was studied using TEM and optical microscopy.

3. Results

3.1. Pre-amorphization of the damaged layer (step 1 and 2)

Pinero et al. [23] previously published a TEM study of hydrogen implantation amorphization of diamond, with the same implantation and annealing parameters used in this study. It was established that the MD and HD conditions cause diamond amorphization after annealing whereas the LD condition does not. ToF-SIMS hydrogen profiles recorded after steps 1 and 2 for LD, MD and HD HPHT samples are given in Fig. 1b, c and d respectively. MD and HD SIMS profiles have been adjusted, so the hydrogen peak concentration is located in the amorphous region observed by the TEM cross-sections shown if Fig. 1e and f. LD depth profile was set the same as MD since no TEM images are available on this sample. More informations on the TEM preparation and analysis can be found in a previous publication [23]. LD SIMS profile was arbitrarily adjusted to the same depth as MD since no amorphous region is present after annealing. Moreover, since loss of detected hydrogen may occur after step 2 annealing, the relative sensitivity factor (RSF) was calibrated using the H concentration in LD. That is to say, the RSF of SIMS profiles acquired after step 2 are adjusted so the total dose in LD condition is 5×10^{16} cm^{-2}. For LD and MD implantation conditions, no significant change in the H concentration peaks is observed after annealing. This indicates that hydrogen exodiffusion is extremely limited in diamond, even after a high temperature annealing at 1000 °C.

One can notice however that HD profile is truncated after step 2. This phenomenon has already been observed in hydrogen-implanted silicon and has been attributed to the presence of molecular hydrogen H_2 [25]. ToF-SIMS technique is not efficient at detecting gaseous molecules due to their volatile nature. Only a small fraction of them remains on the surface to be ionized by the SIMS ion beam, while the rest escape in the chamber in a non-ionized, molecular form. Most H_2 molecules are thus left undetected by the mass spectrometer. This is then a strong indication of the presence of gas-filled nano-cavities, which are the starting point of fractures in the Smart Cut™ technique. Yet, it seems that in these
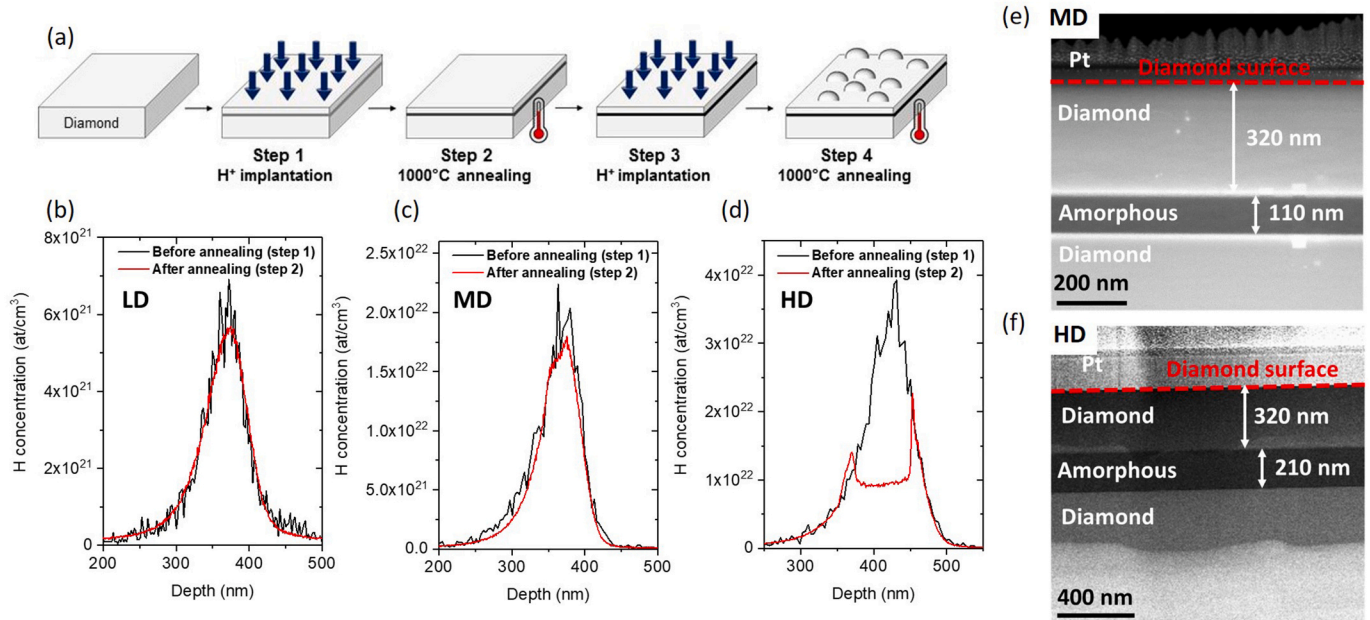
Fig. 1. (a) Schematic of different technological steps used for the blistering process. Doses used in step 1 are detailed in Table I. Step 3 implantation is done at a fixed dose of 2.3×10^{17} cm^{-2}. (a), (b) and (c), ToF-SIMS hydrogen profiles of respectively LD, MD and HD samples after step 1 implantation in black and after step 2 annealing in red. (e) and (f), HAADF micrography of a FIB lamella prepared in respectively the MD and HD sample.

conditions the fraction of molecular hydrogen is too weak to cause an observable blistering. By comparing the HD profiles after step 1 and step 2, the detected hydrogen concentration decreases by about 40% after annealing. Assuming that all the undetected hydrogen is under molecular form, this amount may be insufficient to induce blistering. For example, in silicon it was reported that 60% of the implanted hydrogen is in molecular form [25] when blistering is observed. Moreover, no nano-cavities could be detected by HAADF observation of a lamella taken from the HD sample, shown in Fig. 1 f. Only an homogeneous amorphous, sp^2-rich region is observed. This discrepancy between ToF-SIMS and TEM could be explained by local nano-cavities formation. The area analyzed by ToF-SIMS was a 50×50 μm^2 square, while the region observed on the lamella by HAADF was only a few μm long and between 100 and 200 nm thick. Local nano-cavities and cracks propagation, probably triggered by pre-existing local crystalline defects such as dislocations, could also explain why only two blisters were observed after annealing of the HD sample. Despite this fraction of implanted hydrogen appearing to be converted in dihydrogen in the region probed by ToF-SIMS, significant blistering was not obtained in this area. Even for a higher implanted dose of 4×10^{17} cm^{-2} (not shown in this work), only scarce and local blisters were observed.

To clarify the role of the implanted hydrogen on the diamond crystalline structure, an optical study has been carried out by optical transmission and cathodoluminescence on LD, MD and HD sample, as well as on an unimplanted one, after steps 1 and 2. All spectra are shown in Fig. 2. The cathodoluminescence spectra were recorded scanning a 25 μm^2 area at 7 K, with a beam acceleration voltage of 10 kV and beam current of 10 nA.

At step 1, all three implanted samples exhibit an increased visible light absorption. The strong absorption at high energy (200–300 nm) has been previously attributed to the presence of sp^2 carbon [26]. GR1 center is also detected in both transmission and cathodoluminesence spectra of implanted samples, respectively at 650 nm and 1.675 eV. It is the signature of isolated neutral vacancies (V^0) [27,28]. In cathodoluminescence spectrum, another centre is detected at 2.565 eV and may be attributed to substitutional nickel or to a defect created after neutron irradiation [29]. Finally, cathodoluminescence spectra shows two large peaks centered at 2.2 eV and 3.14 eV. The first one, common to

the four samples, is the signature of boron doping (green band, [28]) and the second one, only detected in the implanted samples has been attributed to boron passivation (blue band, [28]).

At step 1, hydrogen is therefore not detected in any H—V or molecular form but is rather trapped by non-radiative defects. At the same time, V^0 are created and a fraction of sp^3 carbon converts into sp^2 hybridization.

After the first annealing (step 2), all three implanted samples cathodoluminescence spectra exhibit the same features, except for the large signal intensity difference. However, their transmission spectra differ significantly. In a previous study [23], TEM images demonstrated a partial crystalline recovery for LD sample and an amorphous layer formation for MD and HD samples.

The cathodoluminescence study reveals that the peaks related to isolated vacancies and proton implantation damage disappeared after annealing. However, two new peaks and their phonon replica are detected at 2.423 eV and 2.99 eV and are respectively attributed to a defect probably containing interstitial and to N$_3$—V (the N3 centre) [29]. The green band and the blue band remain after annealing but their contribution is hard to define, partly hidden by the other peaks contributions. However, the blue band, undetected in unimplanted sample before annealing appears afterward. The increase of the signal intensity after annealing is attributed to partial crystallinity recovery within the implanted layer. This effect is more pronounced in the LD sample where the opaque amorphous layer is almost fully healed to a colorless diamond, hence the signal intensity is close to the unimplanted sample.

In optical transmission, all implanted samples undergo substantial color change during annealing, while no significant change is observed on the unimplanted one. Overall, three trends are observed depending on the defect density generated during implantation.

(i) At LD, the transmission is significantly increased after annealing, close to the unimplanted condition. Also, the previously observed GR1 centre and sp^2 carbon signature are not detectable anymore. This results are in good agreement with the TEM study of Pinero et al. [23], showing recovering of the crystalline structure.

(ii) At MD, the transmitted light intensity is only slightly increased after annealing. Therefore, the crystalline recovery is only partial.
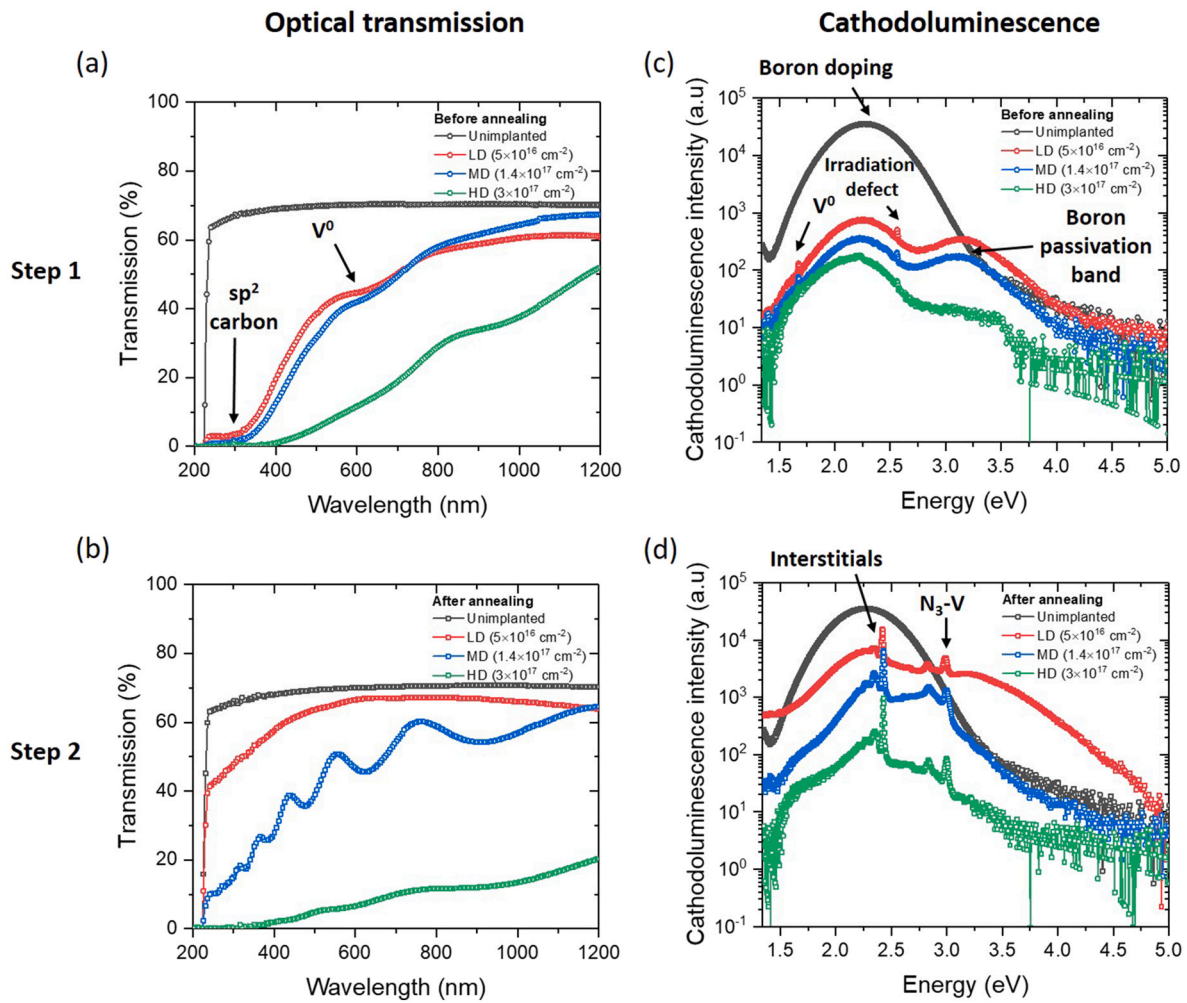
Fig. 2. Optical transmission spectra of unimplanted, LD, MD and HD samples (in gray, red, blue and green respectively) (a) after step 1 and (b) after step 2. Cathodoluminescence spectra of unimplanted, LD, MD and HD samples (in gray, red, blue and green respectively) (c) after step 1 and (d) after step 2. Black arrays show detected defect centers.

The sp^2 carbon signature is not distinctively observed anymore as well as the GR1 center, but an interference pattern may cover its presence. This interference pattern is the signature of a thin, well-defined, absorbing layer [27].

(iii) Finally at HD, the sample seems to keep its pre-annealing features with an overall increased absorption, related to the thickening and/or change of optical properties of the sp^2 rich amorphous layer.

These studies indicate that for a generated defect density of 2×10^{22} cm^{-3} (LD) and lower, the initial amorphous layer can be healed with an annealing. The implanted hydrogen is therefore not able to diffuse and coalesce in H$_2$ molecules. For a defect density of 5.6×10^{22} cm^{-3} (MD), a threshold is crossed over which the implanted layer cannot recover its crystallinity after annealing. Instead, this heavily damaged layer is further enriched in sp^2. It results in a sharp transition, previously reported to be 20 nm [23], between the crystalline and amorphous layers after annealing. It is however important to emphasize that defect densities simulated by SRIM are calculated for a material at 0 K. Thus, SRIM vacancies' density is over-estimated due to the dynamic annealing effect during implantation. It is also well known that the ion beam can cause significant heating of the samples. As such, different equipment and thermal contacts between the substrate holder and samples can induce significant variations of vacancies density. In addition, due to an over-estimation of electronic stopping power of hydrogen in diamond, the

end-of-range calculated by SRIM and given in [23] is largely under-estimated. We however find these simulations useful for the sake of comparison.

In the amorphous layer, part of the implanted hydrogen is able to diffuse sufficiently to recombine in molecular form, indirectly detected in ToF-SIMS experiments. Since no V—H centres are detected, the remainder may be trapped in optically inactive defects. Secondly, isolated vacancies may diffuse and recombine with impurities to form more complex defects, such as N$_3$—V or interstitial-containing defects.

At this stage, implanted hydrogen is too stable in defects and/or small cavities, thus preventing blistering after step 2. Larger doses above 4×10^{17} cm^{-2} and higher temperature annealing might be required. But such conditions are detrimental for the crystalline quality of the trans-ferred film, as well as the wafer bonding techniques necessary for the Smart Cut™ technology.

3.2. Blistering of the diamond surface (step 4)

To further increase the hydrogen content in the amorphous implanted layer and promote H$_2$ formation, a second set of implantation (step 3) and annealing (step 4) has been carried out on a LakeDiamond sample. The implanted doses B1 and B2 are detailed in Table I. The optical microscopy of the surface in both conditions is shown in Fig. 3 (a). Following the final annealing, significant blistering is observed on the surface implanted with B2 conditions, very likely to be compatible
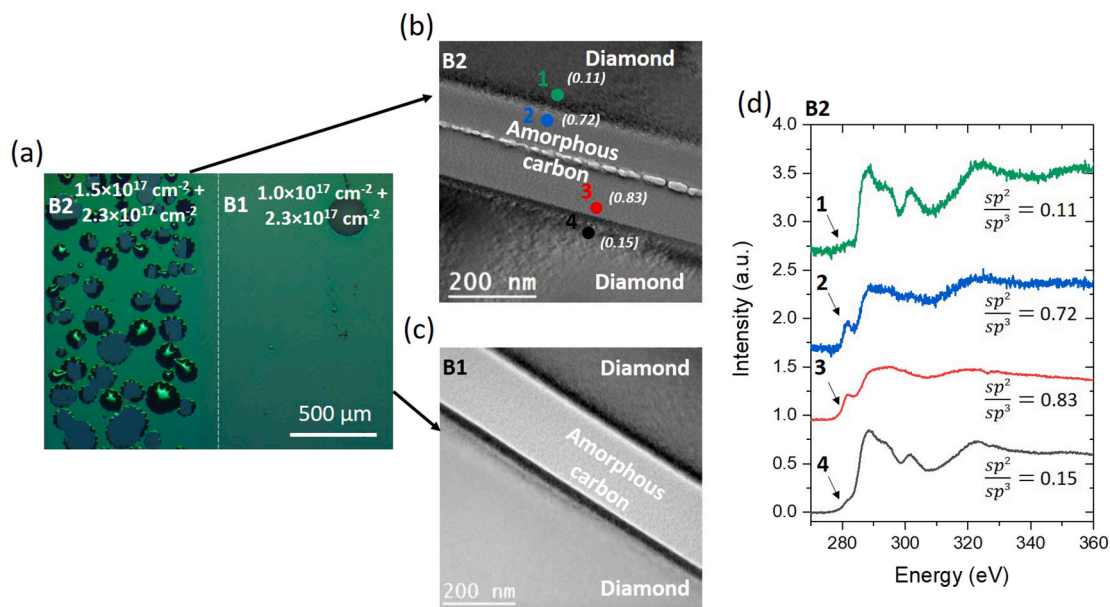
Fig. 3. (a) Optical microscopy of hydrogen implanted sample at $1 \times 10^{17} + 2.3 \times 10^{17}$ cm^{-2} and $1.5 \times 10^{17} + 2.3 \times 10^{17}$ cm^{-2} (B1 and B2 respectively). TEM images of (b) B2 and (c) B1 implanted layers. Locations where STEM-EELS spectra where recorded in B2 are labelled, the extracted sp^2/sp^3 ratios of each area are indicated in parenthesis. (d) STEM-EELS spectra measured from the marked locations in (b) and corresponding sp^2/sp^3 ratios.

with the Smart Cut™ process. In contrast, B1 conditions lead only to local bubbles and exfoliation.

Transmission electron microscopy has been performed in implanted area with B1 and B2 conditions. TEM images are shown in Fig. 3(b) and (c), revealing the presence of the expected amorphous layer in both B1 and B2 condition. The sp^2/sp^3 ratios in crystalline and amorphous carbon layers were extracted from EELS measurements, shown in Fig. 3(d), taken from marked locations in Fig. 3(b). However, nanocavities are only observed using the B2 conditions, in the middle of the amorphous carbon layer. Their expansion and coalescence, due to molecular hydrogen formation are what is causing the macroscopic blistering of the surface. As expected, such feature is not observed in diamond implanted with B1 conditions which did not lead to pre-amorphization. Only an homogeneous amorphous layer is present, similar to one can expect after a single set of implantation and annealing. The desired properties for the pre-amorphized layer are obtained when the generated layer vacancies density is above an amorphization threshold comprised between 2×10^{22} and 5.6×10^{22} cm^{-3} as estimated by SRIM calculation, then annealed at 1000 °C during 1 h to obtain a graphite-like layer.

The need for a pre-amorphization step is quite peculiar to diamond, as in most other material the fracture occurs in a heavily damaged, but crystalline material. One possible explanation is the low diffusivity of hydrogen in diamond, even at high temperature. ToF-SIMS measurements clearly show that after a 1000 °C annealing, there is no significant widening of the hydrogen depth profile. Hydrogen diffusivity is probably too low in the amorphous phase created during implantation as well. While signs of molecular hydrogen cavities formation occur after annealing, at a dose of 3×10^{17} cm^{-2} and higher, no significant blistering was observed up to 4×10^{17} cm^{-2} implanted hydrogen ions (not shown in this work). A large blistered surface is only obtained when an amorphized and annealed layer is hydrogen implanted. In our case, the sp^2/sp^3 ratio increases to reach a value around 0.8 (Fig. 3(d)). Similarly, Kalish et al. [30] reported that after C and Ar implantation above the amorphization threshold and annealing, the amorphous layer becomes graphite-like. Its density drops to around 2.1 cm^{-3} and acquire metallic conduction. It could be that there is a threshold sp^2/sp^3 ratio of the pre-amorphized layer, which allows for sufficient cavities formation for cracks to propagate. Interestingly, Gippius et al. [15] evidenced a "low

temperature" (>800 °C) and a "high temperature" (>1460 °C) graphitisation of hydrogen irradiated diamond. They postulated that with the former, which has been used during pre-amorphization in this work, hydrogen is mostly trapped by radiation damage and the graphitisation is related to vacancies. While in the case of "high temperature" graphitisation, the bonds between hydrogen and the radiation damage are broken, providing free hydrogen able to diffuse, responsible for the observed blistering in their study. One can then suggest that the role of the pre-amorphization is either, to create a layer easier to saturate with hydrogen after a "low temperature" annealing. Or to form a layer in which some of the hydrogen bonds with radiation damage are weaker, such that a "low temperature annealing" can break them. The specific mechanism leading to blistering at >800 °C is yet to be understood.

4. Conclusions

Using two combinations of hydrogen implantation and 1000 °C annealing, blistering conditions have been found. Above a cumulated dose of 3.7×10^{17} cm^{-2} ($1.4 \times 10^{17} + 2.3 \times 10^{17}$ cm^{-2}), gas bubble coalescence happens during last annealing in the centre of the amorphous implanted layer, leading to localized fracture and blistering of the surface. No significant blistering phenomenon occurs after the first annealing: during this step, hydrogen may be trapped in optically inactive defects. For a dose of 3×10^{17} cm^{-2}, signs of nano-cavities formations were nonetheless observed by ToF-SIMS. However, even at a dose as high as 4×10^{17} cm^{-2} and a 1000 °C annealing did not produce blistering. The nano-cavities formation and subsequent cracks propagation seems more favorable when implantation occurs in a sp^2 rich, graphite-like layer, formed by steps 1 and 2 implantation and annealing above the amorphization threshold. This confirms the observation of Suk et al. [22], who also used a pre-amorphization step prior to hydrogen implantation and annealing. These blistering conditions are made at lower temperature than most reported conditions from the literature, could produce a few hundred nanometres thick layers, while preserving the crystallinity of most of the transferred layer. Once combined with wafer bonding, it opens the way to the diamond Smart Cut™.

CRediT authorship contribution statement

Cédric Masante
Writing - Original Draft
Writing - Review & Editing
Formal analysis
Visualization
Jon de Vecchy
Writing - Original Draft
Conceptualization
Methodology
Formal analysis
Investigation
Fédéric Mazen
Methodology
Investigation
Writing - Review & Editing
Frédéric Milési
Investigation
Léa Di Cioccio
Conceptualization
Supervision
Project administration
Julien Pernot
Conceptualization
Supervision
Methodology
Writing - Review & Editing
Fernando Lloret
Investigation
Formal analysis
Daniel Araujo
Investigation
Formal analysis
Jose Carlos Pinero
Writing - Review & Editing
Investigation
Formal analysis
Névine Rochat
Investigation
François Pierre
Investigation
Florence Servant
Supervision
Project administration
Julie Widiez
Conceptualization
Methodology
Supervision
Project administration

Declaration of competing interest

The authors declare that they have no known competing financial interests or personal relationships that could have appeared to influence the work reported in this paper.

References

[1] M. Schreck, S. Gsell, R. Brescia, M. Fischer, Sci. Rep. 7 (2017) 44462.
[2] N.R. Parikh, J.D. Hunn, E. McGucken, M.L. Swanson, C.W. White, R.A. Rudder, D. P. Malta, J.B. Posthill, R.J. Markunas, Appl. Phys. Lett. 61 (1992) 3124.
[3] M. Marchywka, P.E. Pehrsson, D.J. Vestyck, D. Moses, Appl. Phys. Lett. 63 (1993) 3521.
[4] Y. Tzeng, J. Wei, J.T. Woo, W. Lanford, Appl. Phys. Lett. 63 (1993) 2216.
[5] J. Yang, C.F. Wang, E.L. Hu, J.E. Butler, MRS Proc. 956 (2006), https://doi.org/10.1557/PROC-0956-J17-01.
[6] Y. Mokuno, A. Chayahara, H. Yamada, Diam. Relat. Mater. 17 (2008) 415.
[7] Y. Mokuno, A. Chayahara, H. Yamada, N. Tsubouchi, Diam. Relat. Mater. 18 (2009) 1258.
[8] H. Yamada, A. Chayahara, Y. Mokuno, Y. Kato, S. Shikata, Appl. Phys. Lett. 104 (2014), 102110.
[9] E. D. Products, "Excellent Diamond Products website," http://www.d-edp.jp/en/index.html.
[10] M. Bruel, B. Aspar, A.-J. Auberton-Hervé, Jpn. J. Appl. Phys. 36 (1997) 1636.
[11] Soitec, "Soitec website", https://www.soitec.com/fr.
[12] L. Di Cioccio, Y. Le Tiec, F. Letertre, C. Jaussaud, M. Bruel, Electron. Lett. 32 (1996) 1144.
[13] A. Tauzin, T. Akatsu, M. Rabarot, J. Dechamp, M. Zussy, H. Moriceau, J. F. Michaud, A.M. Charvet, L. Di Cioccio, F. Fournel, J. Garrione, B. Faure, F. Letertre, N. Kernevez, Electron. Lett. 41 (2005) 668.
[14] B. Terreault, Phys. Status Solidi A 204 (2007) 2129.
[15] A.A. Gippius, R. Khmelnitskiy, V.A. Dravin, A.V. Khomich, Diam. Relat. Mater. 12 (2003) 538.
[16] A.A. Gippius, R.A. Khmelnitsky, V.A. Dravin, A.V. Khomich, Phys. B Condens. Matter 308 (2001) 573.
[17] V. Popov, L. Safronov, O. Naumova, D. Nikolaev, Y.N. Palyvanov, I.N. Kupriyanov, Nanoscaled semiconductor-on-insulator materials, sensors and devices 276 (2011) 27–33 (Trans Tech Publications.
[18] V. Popov, L. Safronov, O. Naumova, D. Nikolaev, I. Kupriyanov, Y. Palyanov, in: Ion Beam Synthesis and Modification of Nanostructured Materials and Surfaces 282, 2012, p. 100.
[19] Q.-Y. Tong, K. Gutjahr, S. Hopfe, U. Gösele, T.-H. Lee, Appl. Phys. Lett. 70 (1997) 1390.
[20] R. Khmelnitskiy, E. Zavedeev, A. Khomich, A. Gooskov, A. Gippius, Vacuum 78 (2005) 273.
[21] G.F. Kuznetsov, Tech. Phys. 51 (2006) 1367.
[22] J. Suk, H. Kim, W.C. Lim, J. Yune, S. Moon, J.A. Eliades, J. Kim, J. Lee, J. Song, Appl. Phys. Lett. 110 (2017), 101903.
[23] J. Piñero, J. de Vecchy, D. Fernández, G. Alba, J. Widiez, L. Di Cioccio, F. Lloret, D. Araujo, J. Pernot, Appl. Surf. Sci. 528 (2020) 146998.
[24] J. F. Ziegler, "Dedicated website to SRIM", https://www.srim.org.
[25] S. Personnic, K.K. Bourdelle, F. Letertre, A. Tauzin, N. Cherkashin, A. Claverie, R. Fortunier, H. Klocker, J. Appl. Phys. 103 (2008), 023508.
[26] A.T. Collins, P.M. Spear, J. Phys. C Solid State Phys. 16 (1983) 963.
[27] A.V. Khomich, R.A. Khmelnitskiy, V.A. Dravin, A.A. Gippius, E.V. Zavedeev, I. I. Vlasov, Phys. Solid State 49 (2007) 1661.
[28] C. Piccirillo, A. Mainwood, A.T. Collins, M.E. Newton, R. Kalish, in: Diamond and Related Materials 14th European Conference on Diamond, Diamond-Like Materials, Carbon Nanotubes, Nitrides and Silicon Carbide 13, 2004, p. 944.
[29] A. M. Zaitsev, Optical Properties of Diamond (Springer, Berlin Heidelberg).
[30] R. Kalish, A. Reznik, K. Nugent, S. Prawer, Nucl. Instrum. Methods Phys. Res., Sect. B 148 (1999) 626.